PEGylated $MoSe_2$ Nanomaterials with Limited Oxidation via Femtosecond Laser Ablation for Photothermal Therapy

Fan Ye,[†, ‡, §] Holly M. Fruehwald,[||] Kaili Tian,[§] Mohamad Zandieh,[||] Rodney Smith,[‡,||] Joseph Sanderson,[§] Kevin P. Musselman[†, ‡]*

†: Department of Mechanical and Mechatronics Engineering, University of Waterloo, 200 University Ave. West, Waterloo, ON N2L 3G1 Canada

‡: Waterloo Institute for Nanotechnology, 200 University Ave. West, Waterloo, ON N2L 3G1 Canada

§: Department of Physics and Astronomy, University of Waterloo, 200 University Ave. West, Waterloo, ON N2L 3G1 Canada

||: Department of Chemistry, University of Waterloo, 200 University Ave. West, Waterloo, ON N2L 3G1 Canada

* Corresponding author. E-mail: kevin.musselman@uwaterloo.ca

ABSTRACT: $MoSe_2$ nanomaterials are promising photothermal agents for non-invasive cancer treatment. Their surfaces usually need to be functionalized with biocompatible polymers to improve their biocompatibility and colloidal stability and to reduce their cytotoxicity. Herein PEGylated $MoSe_2$ nanomaterials are produced by femtosecond laser ablation of $MoSe_2$ powder in aqueous polyethylene glycol (PEG) solutions. Quantum dots are produced by laser ablation for 30 min with a power of 1.5 W, while larger spherical nanoparticles are produced by laser ablation for 10 min with various powers. PEG molecules attach to the nanomaterials through both physical absorption and Mo-O chemical bonds. A higher concentration of PEG in the solution results in more PEG being attached and increasing the laser ablation power leads to more PEG molecules being attached through chemical bonds. Notably, the attachment of PEG to the nanomaterials through Mo-O bonds can efficiently suppress the oxidation of the $MoSe_2$ nanomaterials to MoO_3 nanoparticles. Both the $MoSe_2$ quantum dots and spherical nanoparticles demonstrate high photothermal conversion efficiencies (PTCEs) and the PTCEs of the quantum dots are overall higher than those of the nanoparticles, making them a promising candidate agent for photothermal cancer therapy.

KEYWORDS: pulsed laser ablation, photothermal, laser-matter interaction, in-situ functionalization, oxidation suppression, polyethylene glycol, molybdenum selenide

Introduction

Photothermal therapy is a non-invasive cancer treatment that uses near infrared (NIR) light to irradiate tumor cells where nanomaterials accumulate, absorb the light energy and convert it to heat to kill the cells. These nanomaterials are also known as photothermal therapy agents (PTAs). In the past decade, transition metal dichalcogenide (TMDC) nanomaterials including

MoS_2,[1–5] WS_2,[6–9] $MoSe_2$,[10–13] WSe_2[14,15] and $MoTe_2$[16] have been widely researched as promising PTAs owing to their high absorbance of NIR light, high specific surface-to-volume ratio and easy surface functionalization, which make them not only good PTAs but also drug carriers for synergistic therapy. However, TMDC nanomaterials need to be surface functionalized with biocompatible polymers to improve their physiological stability and biocompatibility. One way to attach biocompatible polymers is using van der Waals forces. For example, soybean phospholipid, chitosan, polyethylene glycol (PEG), polyvinylpyrrolidone, polyethylene imine (PEI) and F-127 were attached to TMDC nanomaterials *via* van der Waals forces.[5,8,9,11–13,17–20] Another way to conjugate TMDC nanomaterials with biocompatible polymers is through chemical bonds. TMDC nanomaterials can be conjugated with the polymers terminated with lipoic acid groups, such as LA-PEG, and LA-PEI by forming metal-sulfur bonds.[2,3,21–23] All these methods needs hours or even days of stirring of nanomaterials and biocompatible polymers together. Therefore, there exists a need to shorten the surface functionalization time.

Recently, pulsed laser ablation in liquid (PLAL) was proven to be an efficient, simple and green method to prepare TMDC nanomaterials including quantum dots and spherical nanoparticles.[24–30] PLAL involves irradiating femtosecond-laser or nanosecond-laser beams on bulk targets or powders in various solvents. The nanomaterials are usually fragmented from the ablated materials *via* photothermal mechanisms such as spallation, thermodynamic equilibrium melting and vaporization and explosive boiling or direct, intense laser electric field - matter interactions such as Coulomb explosion and photoexfoliation, depending on the intensity and the pulse duration of the laser beam.[31] The nanomaterials are usually stable in the ablated liquid thanks to surface-attached radicals such as hydroxyl groups when laser ablated in water, ethanol, and ethylene glycol.[24,27] The hydroxyl groups result in a negatively charged surface that prevents

aggregation and sedimentation.[27] Additionally, laser-synthesized nanomaterials can be surface functionalized with polymers *in-situ* when ablating target materials and the polymers together. Tsuji et al. prepared silver nanoparticles surface functionalized with polyvinylpyrrolidone (PVP) by laser ablation of a silver plate in aqueous PVP solutions.[32] The silver nanoparticles prepared in PVP solutions were better dispersed than the nanoparticles prepared in pure water.[32] Recently, Haladu et al. reported the synthesis of silver quantum dots surface functionalized with polyaspatate (PASP) for antimicrobial applications by laser ablation of a silver plate in PASP aqueous solutions.[33] Choi et al. also synthesized PVP coated aluminum nanoparticles by laser ablation of an aluminum plate in PVP aqueous solutions.[34] It was found that the surface attachment of PVP prevented the aggregation of the nanoparticles, improved the colloidal stability, and minimized the hydroxylation of the nanoparticles in prolonged ablation.[34] Additionally, colloidally stable gold nanoparticles could also be prepared in aqueous solutions containing surfactant polymers such as cetyl-trimethylammonium bromide and sodium dodecyl sulfate.[35,36] Moreover, nanomaterials prepared by PLAL in oxygen containing solvents, especially water, are easily oxidized.[24,25,29,37,38] Sometimes the formation of oxide coatings or carbon coatings on nanoparticles can protect the nanoparticles from further oxidation. It was reported that the *in-situ* formation of surface aluminum oxide coatings on aluminum nanoparticles during femtosecond laser ablation of aluminum pellets in ethanol can prevent further oxidation of the nanoparticles.[39] Similarly, the formation of graphite coatings on iron nanoparticles during femtosecond laser ablation of an iron target in acetone also prevented further oxidation.[40] However, there have been no reports about *in-situ* surface functionalization of biocompatible polymers and preventing oxidation of TMDC nanomaterials during pulsed laser ablation in oxygen-containing solvents.

In this work, a facile synthesis method is developed to prepare $MoSe_2$ nanomaterials including quantum dots and larger spherical nanoparticles and simultaneously functionalize them *in-situ* with PEG by femtosecond laser ablation of $MoSe_2$ powder in aqueous PEG solutions. High-power and long-time laser ablation yields $MoSe_2$ quantum dots, with the oxidation of the quantum dots being suppressed as the concentration of PEG in the solutions increases. In contrast, laser ablation conducted in water or a solution with a low concentration of PEG (0.0625 mg/mL) results in the oxidation of the $MoSe_2$ powder into MoO_3 nanoparticles. Short-time ablation results in the formation of spherical nanoparticles. PEG molecules can attach to the nanoparticles *via* van der Waals forces or chemical bonds. High-power laser ablation results in more PEG attached to the nanoparticles *via* Mo-O chemical bonds, preventing the nanoparticles from further oxidation. Both the PEGylated $MoSe_2$ quantum dots and the spherical nanoparticles exhibit high photothermal conversion efficiency (PTCE), but the PTCE of the $MoSe_2$ quantum dots are overall higher than those of the $MoSe_2$ spherical nanoparticles, making them potential photothermal therapy agents for non-invasive cancer treatment.

Experimental Methods

Synthesis of PEGylated $MoSe_2$ Nanomaterials

PEG (4000 MW, Sigma-Aldrich) was added to deionized water to prepare PEG solutions with different concentrations of 0.0625 mg/mL, 0.125 mg/mL, 0.25 mg/mL, 0.5 mg/mL and 1 mg/mL. After complete dissolution of the PEG in water, $MoSe_2$ powder (99.9%, 325 mesh, Thermo Scientific) with a concentration of 1.1 mM was added into each solution. After 20 min of bath sonication to break agglomerates, 4 mL of the suspension sample was transferred to a small vial for laser ablation. The small vial was placed on a magnetic-stirrer plate and a NIR laser beam (wavelength: 800 nm, pulse duration: 35 fs, repetition rate: 1 kHz, beam diameter: 1

cm, beam quality (M2): ⩽1.3, Model: Spitfire Ace-35F) was focused into the sample with a 5 cm-focal-length plano-convex lens. The average power of the incident laser was varied to be 0.15 W, 0.3 W, 0.6 W and 1.5 W using a half-wave plate and a polarizing beam splitter. The suspension was stirred at 300 rpm during laser ablation. After laser ablation, the solutions were dialyzed against deionized water for 3 days to remove extra PEG.

Characterization of Nanomaterials

A Zeiss Libra 200MC high resolution transmission electron microscopy (HRTEM) operating at 200 kV was used to observe the shapes and microstructures of the laser-synthesized nanomaterials. Grazing incidence X-ray diffraction (GIXRD) with Cu Kα radiation was carried out using a PANalytical X'Pert Pro MRD diffractometer to identify the phases of the nanomaterials. The Raman spectra of the nanomaterials were measured with a Renishaw micro-Raman spectrometer (laser wavelength of 532 nm). The X-ray photoelectron spectroscopy (XPS) spectra of the nanomaterials were obtained using a Thermo VG Scientific ESCALab 250 microprobe with Monochromatic Al Kα excitation (1486.6 eV). The surface attachment of PEG to the nanoparticles was analyzed by a Bruker Tensor 27 Fourier transform infrared (FTIR) spectrometer with attenuated total reflection (ATR) mode. The thermogravimetric analysis (TGA) curves of pure PEG and the PEGylated $MoSe_2$ nanomaterials after freeze drying were recorded using a TA Instruments TGA Q500 with a ramp rate of 10 °C/min. The absorbance spectra of the nanomaterials were measured with a UV-vis-NIR spectrometer (Lambda 1050, PerkinElmer). The PTCEs of the nanoparticles were evaluated using a custom-built setup, as described in the previous work.[30,38,41] The concentration of $MoSe_2$ in all the samples was 1.1 mM. 1 mL of each sample was transferred to a quartz cuvette with a path length of 1 cm, and then illuminated by an 808 nm continuous-wave laser (BWF1-B&W Tek) for 10 min followed

by cooling for 10 min. The temperatures of the solvent and the environment were recorded by two thermocouples (Fisherbrand) placed inside and outside the cuvette, respectively. The calculation of the PTCEs of the samples is detailed in S1, Supporting Information.

Results and Discussion

Influence of Concentration of PEG

Figure 1a-f shows TEM images of nanomaterials prepared by femtosecond laser ablation in water with different concentrations of PEG for 30 min at 1.5 W. The nanomaterials were dialysed against deionized water to remove extra PEG molecules after laser ablation. When the concentration of PEG is higher than 0.125 mg/mL, as shown in **Figure 1a-d**, quantum dots with lattice spacing of 2.89 Å corresponding to (100) planes of $MoSe_2$ are observed. This is consistent with previous research that long-time ablation with high-power laser pulses leads to the formation of quantum dots which are fragmented from ablated materials *via* Coulomb explosion and explosive boiling.[25,29,37] Instead of quantum dots, larger spherical nanoparticles are observed in **Figure 1e and f**. **Figure 1e** shows a nanoparticle prepared in 0.0625 mg/mL PEG solution; it has a lattice spacing of 3.21 Å corresponding to (011) planes of MoO_3. **Figure 1f** shows a nanoparticle prepared in pure water; it has a lattice spacing of 3.52 Å corresponding to (002) planes of MoO_3. This suggests that $MoSe_2$ was oxidized into MoO_3 when laser ablated in water or the solution with a low concentration of PEG. The size distributions of the quantum dots are presented in **Figure S1**. The mean size of the dots is around 3.8 nm when the concentration of PEG ranges from 0.125 mg/mL to 0.5 mg/mL and drops slightly to 3.4 nm when the concentration of PEG increases to 1 mg/mL. The drop in size might be caused by an increased amount of PEG attached to the quantum dots, which blocked further aggregation of fragmented ions, atoms, or nanoclusters. The XRD patterns of the nanomaterials prepared in water and PEG

solutions (0.125 mg/mL, 0.5 mg/mL, and 1 mg/mL) are shown in **Figure S2**. The sample prepared in water shows (002), (011) and (110) peaks of MoO_3 and a small (002) peak of $MoSe_2$, suggesting that the nanomaterial was mainly oxidized, consistent with the observation in the TEM image (**Figure 1f**). In contrast, the samples prepared in PEG solutions mainly show a small (002) peak of $MoSe_2$, implying the addition of PEG with concentrations higher than 0.125 mg/mL can efficiently protect $MoSe_2$ from oxidation during laser ablation.

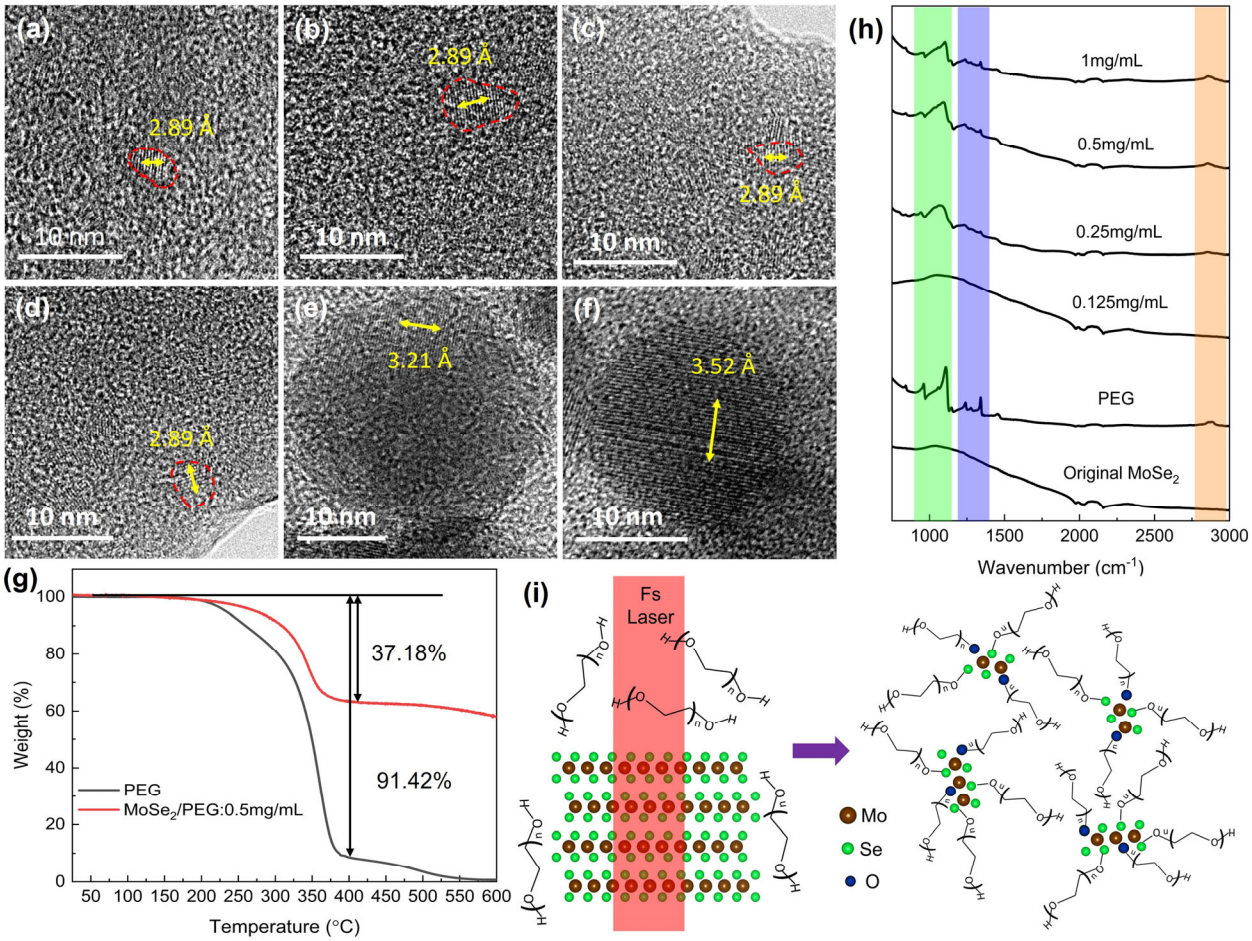

Figure 1. TEM images of nanomaterials prepared by femtosecond laser ablation (30 min at 1.5 W) of $MoSe_2$ powder in PEG solutions with different concentrations of (a) 1 mg/mL, (b) 0.5 mg/mL, (c) 0.25 mg/mL, (d) 0.125 mg/mL, (e) 0.0625 mg/mL and (f) pure water. (g) TGA

curves of PEG powder and PEGylated $MoSe_2$ quantum dots prepared in the 0.5 mg/mL PEG solution. (h) ATR-FTIR spectra of original MoSe2 powder, PEG, and quantum dots prepared in PEG solutions with different concentrations for 30 min at 1.5 W. The peaks are assigned to C-O stretching vibration modes (green shade), C-H bending vibration modes (blue shade), and C-H stretching vibration modes (orange shade). (i) Schematic diagram of the laser ablation process, showing attachment of PEG molecules to the $MoSe_2$ quantum dots.

Figure 1g shows the TGA curves of PEG powder and PEGylated $MoSe_2$ quantum dots prepared in the 0.5 mg/mL PEG solution *via* laser ablation for 30 min at 1.5 W. The PEGylated $MoSe_2$ sample was prepared by freeze drying after dialysis against water to remove excess PEG. The weight of pure PEG drops by 91.42% when the temperature increases from 25 °C to 400 °C due to decomposition. The weight of the PEGylated $MoSe_2$ quantum dots drops by 37.18% in the same temperature range, which is attributed to decomposition of the PEG. The FTIR spectra of the original $MoSe_2$, PEG and PEGylated $MoSe_2$ quantum dots are shown in **Figure 1h**. The original $MoSe_2$ powder has no active FTIR peaks. PEG has a major peak at 1108 cm^{-1} assigned to C-O stretching vibration, peaks at 1233 cm^{-1} and 1343 cm^{-1} assigned to C-H symmetric and asymmetric bending vibrations, and a peak at 2873 cm^{-1} assigned to C-H stretching vibration.[42] The $MoSe_2$ quantum dots prepared in PEG solutions with concentrations ranging from 0.25 mg/mL to 1 mg/mL all show PEG peaks, suggesting the surface attachment of PEG. The sample prepared in 0.125 mg/mL PEG solution doesn't show PEG peaks, probably because the amount of the attached PEG was too low to be detected. Both the TGA and FTIR results suggested that PEG molecules were successfully attached to the $MoSe_2$ quantum dots during laser ablation (**Figure 1i**).

Figure 2a-g displays the Mo3d XPS spectra of the original $MoSe_2$ powder and the quantum dots prepared in PEG solutions with varying concentrations using laser ablation for 30 min at 1.5 W. The original $MoSe_2$ powder (**Figure 2a**) exhibits two peaks at 228.9 eV and 232.1 eV assigned to $Mo3d_{5/2}$ and $Mo3d_{3/2}$ of $MoSe_2$. The nanoparticles prepared in pure water (**Figure 2b**) display two peaks at 232.9 eV and 235.9 eV assigned to $Mo3d_{5/2}$ and $Mo3d_{3/2}$ of Mo(VI)-O bonds, suggesting significant oxidation of $MoSe_2$ to MoO_3. In addition to the $MoSe_2$ and MoO_3 peaks, the nanoparticles prepared in the 0.0625 mg/mL PEG solution (**Figure 2c**) exhibit two other small peaks at 230.3 eV and 232.7 eV, corresponding to $Mo3d_{5/2}$ and $Mo3d_{3/2}$ of Mo(IV)-O bonds.[43,44] The high MoO_3 peaks in the nanoparticles prepared in the 0.0625 mg/mL PEG solution imply the nanoparticles were also significantly oxidized during laser ablation, consistent with the TEM image (**Figure 1e**). When the PEG concentration is 0.125 mg/mL or higher (**Figure 3d-g**), high $MoSe_2$ peaks and decreased Mo(VI)-O peaks suggest suppressed oxidation in the $MoSe_2$ quantum dots. **Figure 2h** shows the decreased contribution of the Mo(VI)-O bond in the $MoSe_2$ quantum dots with increasing concentration of PEG. However, the Mo(IV)-O content remains consistent in all the samples prepared in solutions with PEG concentration no less than 0.125 mg/mL, slightly decreasing only in the 0.5 mg/mL PEG sample. The decrease might be attributed to the suppressed oxidation as the Mo(VI)-O content also decreases. However, the Mo(IV)-O content increases slightly in the 1 mg/mL PEG sample, while the Mo(VI)-O content continues decreasing. This might be caused by increased surface attachment of PEG to the quantum dots *via* Mo(IV)-O bonds, suggesting that the Mo(IV)-O bond is not only caused by partial oxidation but also surface attachment of PEG *via* chemical bonds. Laser ablation can simultaneously ionize and fragment PEG during $MoSe_2$ powder fragmentation such that the ionized PEG can bond with the fragmented $MoSe_2$ through

chemical bonds. **Figure S3** shows the C1s XPS spectra of the original $MoSe_2$ powder and nanomaterials prepared in pure water and PEG solutions with different concentrations. All the samples exhibit a peak at 285 eV assigned to C-C bonds and a peak at 286.6 eV assigned to C-O bonds.[45] The height of the C-O peak in the $MoSe_2$ quantum dots was found to increase with increasing PEG concentration, implying greater attachment of PEG molecules to the quantum dots during laser ablation.[45]

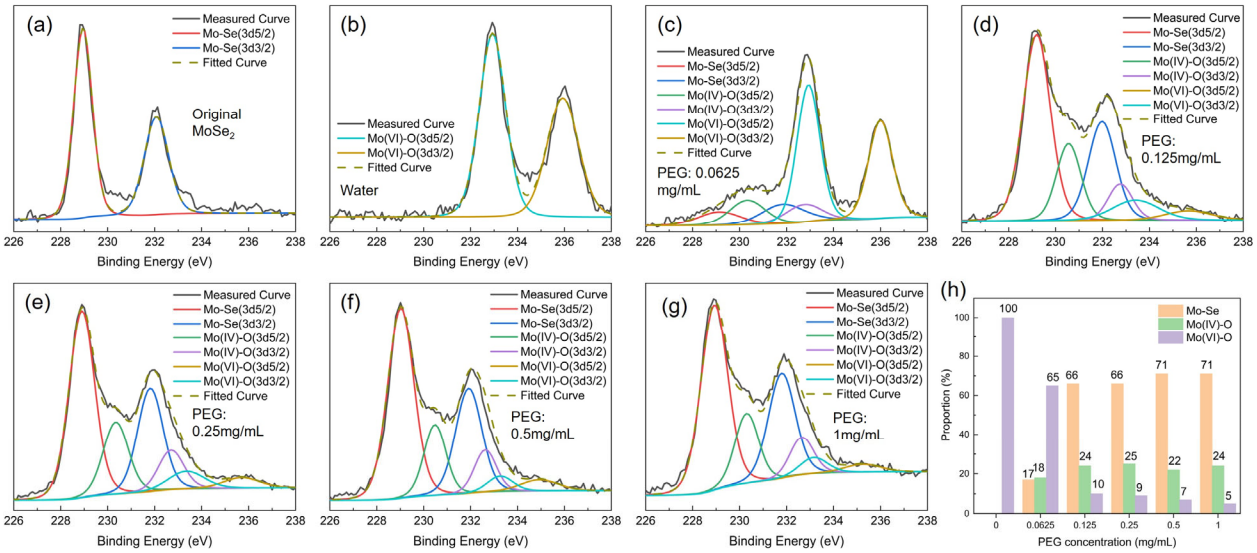

Figure 2. Mo3d XPS spectra of (a) original $MoSe_2$ powder and nanomaterials prepared in (b) pure water and PEG solutions with concentrations of (c) 0.0625 mg/mL, (d) 0.125 mg/mL, (e) 0.25 mg/mL, (f) 0.5 mg/mL and (g) 1 mg/mL for 30 min at 1.5 W. (h) Proportions of Mo-Se, Mo(IV)-O, and Mo(VI)-O bonds in the nanomaterials prepared in aqueous solutions with different concentrations of PEG.

Figure 3 shows the Raman spectra of the original $MoSe_2$ powder and nanomaterials prepared in pure water and PEG solutions with different concentrations for 30 min at 1.5 W. The original $MoSe_2$ powder has a peak at 241 cm^{-1} assigned to the A_{1g} vibration mode. This peak disappears in the nanoparticles prepared in pure water and the 0.0625 mg/mL PEG solution.

Instead, another two peaks located at 796 cm^{-1} and 962 cm^{-1}, which are assigned to Mo-O stretching modes of molybdenum oxide, appear.[46,47] This is consistent with the TEM images (**Figure 1e and f**) and the XPS spectra (**Figure 2b and c**). The quantum dots prepared in the PEG solutions with concentrations no less than 0.125 mg/mL have a primary peak at 255 cm^{-1} (blue dashed line in **Figure 2a**) in addition to the A_{1g} peak of $MoSe_2$ (red dashed line in **Figure 2a**). The peak at 255 cm^{-1} is probably attributable to blueshifting of the A_{1g} peak of oxygen-doped $MoSe_2$ ($MoSe_{2-x}O_x$), which might be formed by partial oxidation and the attachment of PEG to the quantum dots *via* Mo-O bonds during laser ablation. Blueshifting of the A_{1g} peak was previously reported in oxygen-doped MoS_2.[48,49]

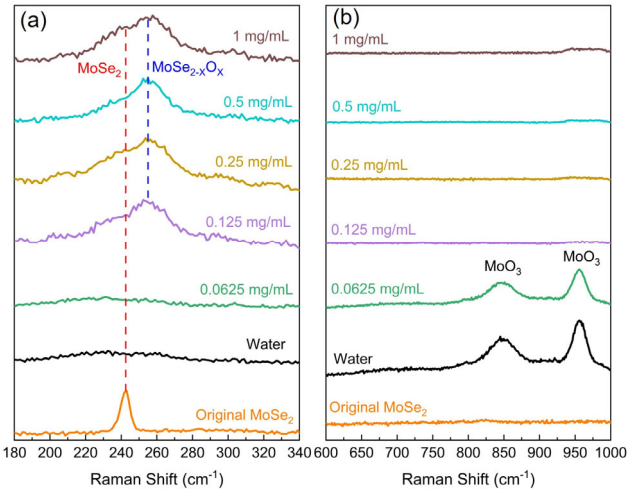

Figure 3. Raman spectra ranging (a) from 180 to 340 cm^{-1} and (b) from 600 to 1000 cm^{-1} of original $MoSe_2$ powder and nanomaterials prepared in pure water and PEG solutions with different concentrations of PEG for 30 min at 1.5 W. The red dashed line denotes the A_{1g} mode of original $MoSe_2$ powder. The blue dashed line denotes the shifted A_{1g} peak of oxygen-doped $MoSe_2$ quantum dots.

Therefore, it can be concluded that the addition of a sufficient concentration of PEG (≥ 0.125 mg/mL) in water during laser ablation of $MoSe_2$ powder can effectively protect the formed quantum dots from oxidation This protection occurs through the surface attachment of PEG to the quantum dots, isolating them from reactive oxygen species created during the laser ablation. Nevertheless, it is evident that a small amount of PEG is insufficient to protect the $MoSe_2$ quantum dots from oxidation, probably due to inadequate coverage.

Influence of Laser Power

The last section has shown that PEG can be attached to $MoSe_2$ quantum dots *via* Mo-O chemical bonds during laser ablation with a high power (1.5W) for a long time (30 min). This section examines if different laser powers can affect the attachment of PEG to $MoSe_2$ nanomaterials. Four different laser powers of 0.15 W, 0.3 W, 0.6 W and 1.5 W were selected to ablate $MoSe_2$ powder dispersed in 0.5 mg/mL aqueous PEG solution for 10 min. **Figure 4** illustrates spherical nanoparticles produced by laser ablation with different powers. This is consistent with our previous work that spherical nanoparticles, rather than quantum dots, are produced using short ablation times.[30] The size distributions of the nanoparticles prepared with different laser powers are presented in **Figure S4**. The nanoparticles prepared with 0.15 W and 0.3 W laser pulses have mean sizes of 26.3 nm and 23.5 nm, respectively, while the nanoparticles prepared with 0.6 W and 1.5 W laser pulses have smaller mean sizes of 14.7 nm and 12.6 nm, respectively. According to our previous work,[30] the large spherical nanoparticles produced in low-power laser ablation are primarily formed by thermodynamic equilibrium melting and evaporation of the ablated particles, while the smaller nanoparticles produced in high-power laser ablation are primarily formed by explosive boiling of the ablated particles.

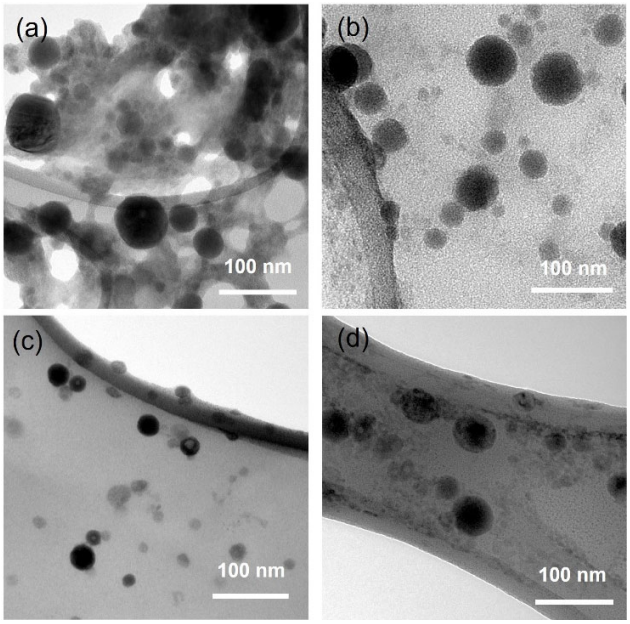

Figure 4. TEM images of nanoparticles prepared by laser ablation in the 0.5 mg/mL PEG solution for 10 min at different powers of (a) 0.15 W, (b) 0.3 W, (c) 0.6 W and (d) 1.5 W.

The Mo3d XPS spectra of the nanoparticles prepared with different laser powers are presented in **Figure 5a-d**. All the nanoparticles display peaks assigned to Mo-Se, Mo(IV)-O, and Mo(VI)-O bonds. The proportions of Mo-Se, Mo(IV)-O and Mo(VI)-O bonds are shown in **Figure 5e**. Notably, the nanoparticles prepared with 0.15 W laser pulses exhibit the highest content of Mo-Se bond but the lowest content of Mo(IV)-O bond. In addition, they also exhibit the highest C-O/C-C ratio (**Figure S5**). The C-O bond is primarily contributed by surface attached PEG whereas the Mo(IV)-O bond is attributed to oxygen doping resulting from partial oxidation and surface attachment of PEG *via* Mo-O chemical bonds. Therefore, the lower content of Mo(IV)-O bond and higher C-O/C-C ratio are reasonably associated to the surface attachment of PEG to the nanoparticles *via* van der Waals forces. When the laser power increases to 0.3 W, there is a rise in both Mo(IV)-O and Mo(VI)-O bond proportions, signifying increased oxidation caused by increased amount of reactive oxygen species as a result of the elevated laser

power. Despite the still high C-O/C-C ratio in **Figure S5**, the escalation in oxidation might be linked to the majority of PEG molecules attaching to the nanoparticles *via* van der Waals forces, unable to effectively suppress oxidation. When the laser power increases above 0.6 W, the content of Mo(IV)-O bond increases whereas the content of Mo(VI)-O bond decreases. This shift might be attributed to increased surface attachment of PEG to the nanoparticles *via* Mo-O chemical bonds, preventing further oxidation of the nanoparticles. Meanwhile, the C-O/C-C ratio decreases with the increased laser power, likely due to the fragmentation of PEG chains in high-power ablation, resulting in shorter PEG molecules which were still capable of protecting the nanoparticles from further oxidation as long as they attached to the nanoparticles *via* chemical bonds. Moreover, it is notable that the nanoparticles prepared with shorter ablation time (1.5 W, 10 min, 0.5 mg/mL PEG) exhibit larger proportion of Mo-O bonds, especially the Mo(IV)-O bond, than the quantum dots prepared with longer ablation time (1.5 W, 30 min, 0.5 mg/mL PEG), when comparing **Figure 2h and 5e**. This might be attributed to the ablation of the surface-attached PEG during prolonged laser ablation, indicated by the lower C-O/C-C ratio observed in the quantum dots prepared through 30 min ablation (**Figure S3f**) compared to those synthesized by 10 min ablation (**Figure S5d**).

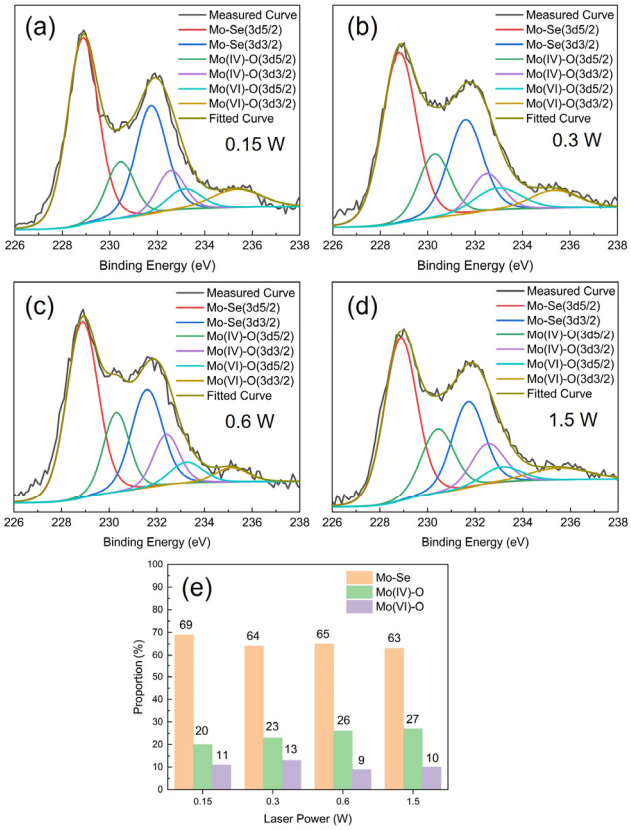

Figure 5. Mo3d XPS spectra of the nanoparticles prepared by laser ablation in the 0.5 mg/mL PEG solution with different powers of (a) 0.15 W, (b) 0.3 W, (c) 0.6 W and (d) 1.5 W for 10 min. (e) Proportions of Mo-Se, Mo(IV)-O, and Mo(VI)-O bonds in the nanoparticles prepared in 0.5 mg/mL PEG solution with different laser powers.

The Raman spectra of the nanoparticles prepared by laser ablation with different powers are shown in **Figure 6**. The nanoparticles prepared with 0.15 W laser pulses exhibit the A_{1g} peak at 241 cm^{-1} (marked with red dashed line). As the laser power increases, there is a gradual decrease in the intensity of this peak, while the intensity of the peak at 255 cm^{-1} (marked with blue dashed line) assigned to the A_{1g} vibration mode of oxygen-doped $MoSe_2$ increases. This observation aligns with the change observed in the proportion of Mo(IV)-O bonds in **Figure 5e**, suggesting

an increased amount of PEG attached to the nanoparticles *via* Mo-O chemical bonds as the laser power increases.

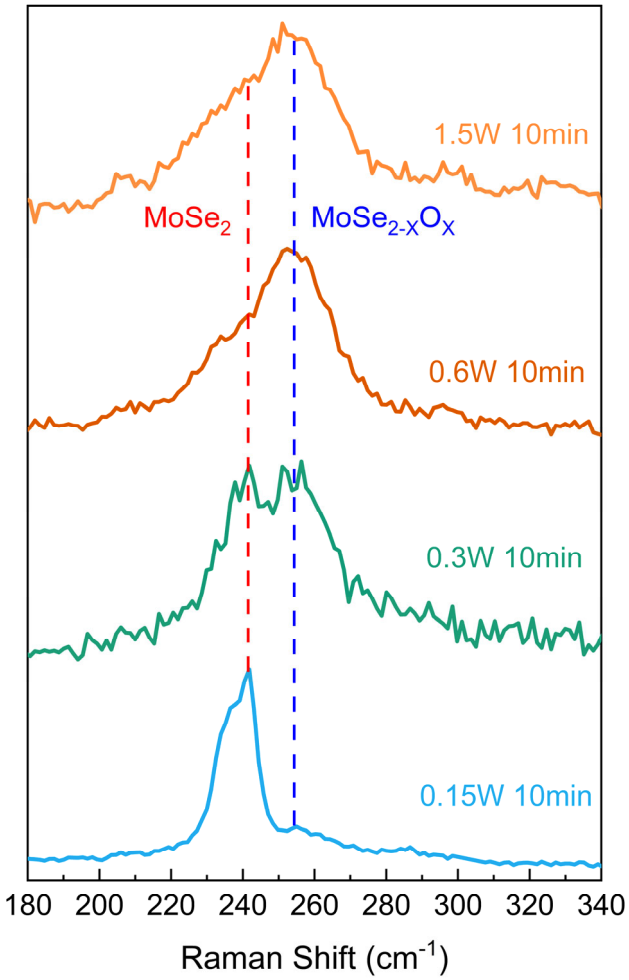

Figure 6. Raman spectra of the nanoparticles prepared by laser ablation in the 0.5 mg/mL PEG solution with different powers for 10 min. The red dashed line denotes the A_{1g} mode of original $MoSe_2$ powder. The blue dashed line denotes the shifted A_{1g} peak of oxygen-doped $MoSe_2$ nanoparticles.

Therefore, it can be inferred that $MoSe_2$ nanoparticles prepared by laser ablation in PEG solutions can attach PEG *via* either van der Waals forces or Mo-O chemical bonds. The increase in laser power led to more PEG attached to the nanoparticles *via* Mo-O chemical bonds, as

described in **Figure 7**, contributing to the prevention of further oxidation of the nanoparticles. Additionally, the length of the PEG molecules attached to the nanoparticles decreased with increasing laser power.

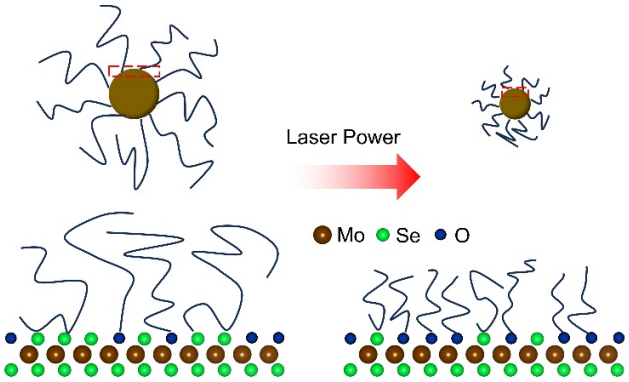

Figure 7. Schematic diagram showing the attachment of PEG to $MoSe_2$ nanoparticles. The surface PEGylation of the nanoparticles marked in red dashed boxes are shown in the bottom figures. With increasing laser power, the nanoparticles become smaller, the length of attached PEG becomes shorter, and more PEG is attached to $MoSe_2$ *via* Mo-O bonds.

Photothermal Conversion Efficiencies of PEGylated $MoSe_2$ Nanomaterials

The PTCEs of the PEGylated $MoSe_2$ nanomaterials were measured using an 808 nm laser at 0.47 W. The concentration of $MoSe_2$ in all the measured samples was 1.1 mM. The sample prepared by laser ablation for 10 min in the 0.5 mg/mL PEG solution with a low laser power of 0.15 W was excluded from measurement due to the presence of significant sediment of unablated bulk powder particles resulting from the low-power and short-time ablation process. **Figure 8a and b** show the temperature changes observed in the measured samples after being illuminated by the 808 nm laser for 10 min followed by cooling for another 10 min.

Figure 8a depicts the temperature changes of the samples prepared in PEG solutions with different PEG concentrations, as well as water and a PEG solution without $MoSe_2$. The temperature of water and the PEG solution (0.5 mg/mL) only increases by 0.7 °C and 0.5 °C, respectively, during a 10 min laser illumination. This suggests that PEG alone had no contribution to the heat generation upon NIR light illumination. Moreover, the samples prepared in pure water and the 0.0625 mg/mL PEG solution also show minor temperature increases of only 0.9 °C and 0.7 °C respectively, since most $MoSe_2$ nanoparticles within the solutions were oxidized into MoO_3, which cannot generate heat upon NIR laser illumination.[38] In contrast, the samples prepared in PEG solutions with concentrations of 0.125 mg/mL, 0.25 mg/mL, 0.5 mg/mL and 1 mg/mL display obvious temperature elevations of 7.5 °C, 9.3 °C, 14 °C and 14.9 °C, respectively. The PTCEs of the $MoSe_2$ quantum dots prepared in PEG solutions with lower concentrations (0.125 mg/mL and 0.25 mg/mL) are around 42.5%, while the PTCEs of the quantum dots prepared in PEG solutions with higher concentrations (0.5 mg/mL and 1 mg/mL) reach around 44%, as depicted in **Table 1**. These PTCE values are in line with those of $MoSe_2$ quantum dots prepared through probe sonication (46.5%),[11] lower than $MoSe_2$ nanoflowers (61.8%),[12] but surpass those of several other TMDC nanomaterials such as MoS_2 (24.4%,[1] 27.6%[2], 25.1%[4], 23.8%[13]), WS_2 (32.8%,[6] 35%[7]), $MoTe_2$ (33.8%),[16] and WSe_2 (35.1%,[14] 38.3%[15]). Given the PTCEs of the quantum dots prepared in different samples are close to each other, the higher temperature increases observed in the samples prepared in 0.5 mg/mL and 1 mg/mL PEG solutions can be attributed to higher NIR light absorption, as shown in **Figure 8c**. The high absorbance might be caused by smaller bandgaps and increased Urbach energies. The bandgaps were obtained from Tauc plots (**Figure S6**). **Table 1** reveals that the quantum dots prepared in 0.125 mg/mL and 0.25 mg/mL PEG solutions possess bandgaps of approximately

1.38 eV, whereas those prepared in 0.5 mg/mL and 1 mg/mL PEG solutions possess lower bandgaps of approximately 1.1 eV. Given the produced quantum dots display very close sizes (**Figure S1**), the larger bandgaps of the quantum dots prepared in the PEG solutions with lower concentrations might stem from more significant oxidation (**Figure 2h**). The Urbach energies of the quantum dots were measured by the method introduced in our previous work,[30] and the plots used to determine the Urbach energies are presented in **Figure S7**. A higher Urbach energy suggests higher sub-bandgap absorption of photons because of an increased density of electronic states extending into the forbidden gap (Urbach tails) as a result of increased lattice disorder or defects in materials. Therefore, the increased Urbach energy with PEG concentration (**Table 1**) is probably caused by increased surface attachment of PEG *via* Mo-O bonds, which increases lattice disorder on the surface of the quantum dots.

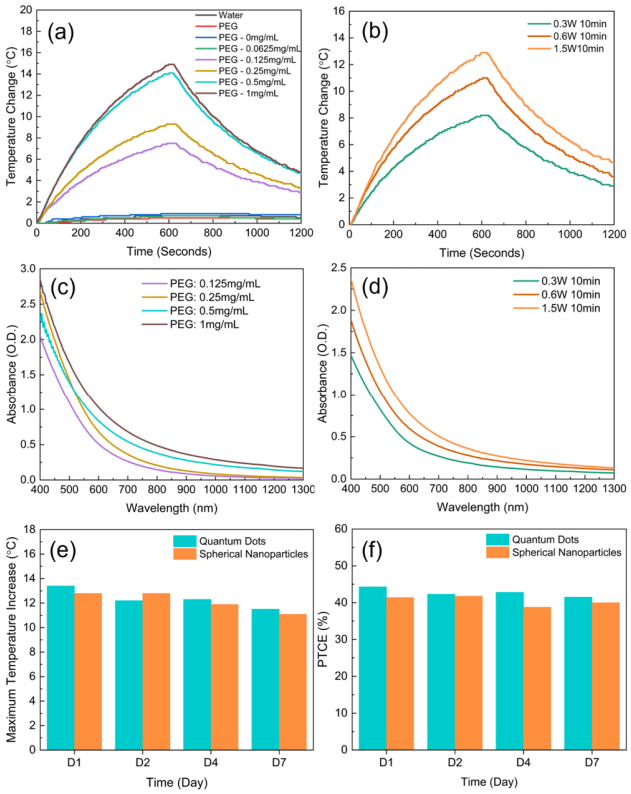

Figure 8. Temperature-change curves of (a) water, PEG solution (0.5 mg/mL) and the quantum dots prepared by laser ablation (1.5 W, 30 min) in water and PEG solutions with different concentrations, and (b) the spherical nanoparticles prepared by laser ablation for 10 min with different laser powers in the 0.5 mg/mL PEG solution after being illuminated by an 808 nm laser beam for 10 min followed by cooling for another 10 min. UV-vis-NIR absorbance spectra of (c) the quantum dots prepared by laser ablation (1.5 W, 30 min) in PEG solutions with different concentrations and (d) the spherical nanoparticles prepared by laser ablation with different laser powers in the 0.5 mg/mL PEG solution. Stability of (e) the maximum temperature increase and (f) PTCE of quantum dots and spherical nanoparticles prepared by laser ablation at 1.5 W for 30 min and 10 min respectively in the 0.5 mg/mL PEG solution.

Table 1. Bandgaps, Urbach energies, maximum temperature increases upon laser illumination and PTCEs of the PEGylated $MoSe_2$ quantum dots prepared by laser ablation for 30 min at 1.5 W in PEG solutions with different concentrations.

PEG Concentration	Bandgap	Urbach Energy	Maximum Temperature Increase	PTCE
0.125mg/mL	1.39eV	0.336eV	7.5°C	42.3%
0.25mg/mL	1.38eV	0.353eV	9.3°C	42.8%
0.5mg/mL	1.08eV	0.564eV	14°C	44.2%
1mg/mL	1.10eV	0.612eV	14.9°C	43.8%

Figure 8b shows that the temperature of the samples prepared in 0.5 mg/mL PEG solution with different laser powers of 0.3 W, 0.6 W and 1.5 W increases by 8.2°C, 10.2°C and 12.9°C, respectively. The PTCE of the $MoSe_2$ nanoparticles increases with the laser ablation power, with the highest PTCE of 40.9% obtained in the sample prepared with 1.5 W laser pulses, as shown in

Table 2. The larger temperature increases in the samples prepared with increasing laser ablation power might be attributable to higher absorbance of NIR light (**Figure 8d**) and the increased PTCE. It is interesting to find in **Table 2** that the nanoparticles prepared with 0.6 W and 1.5 W laser pulses possess bandgaps of 1.25 eV, slightly smaller than those prepared with 0.3 W laser pulses (1.29 eV). The slightly higher bandgap of the nanoparticles prepared with 0.3 W laser pulses might be caused by more oxidation, as indicated in **Figure 5e**. As the bandgaps of the nanoparticles in different samples are close to each other, the increased absorbance of NIR light and PTCE could be attributed to enhanced sub-bandgap absorption of photons and nonradiative recombination of the excited carriers. As shown in **Table 2**, the Urbach energy of the spherical nanoparticles increases with the laser ablation power, in line with our previous research that higher laser ablation power introduces more defects into the nanoparticles, which increases the sub-bandgap absorption and facilitates the non-radiative recombination of excited carriers.[30]

Table 2. Bandgaps, Urbach energies, maximum temperature increases upon laser illumination and PTCEs of PEGylated $MoSe_2$ spherical nanoparticles prepared by laser ablation for 10 min in the 0.5 mg/mL PEG solution with different laser powers.

Laser Power	Bandgap	Urbach Energy	Maximum Temperature Increase	PTCE
0.3 W	1.29eV	0.620eV	8.2°C	36.9%
0.6 W	1.25eV	0.641eV	10.2°C	38.2%
1.5 W	1.25eV	0.663eV	12.9°C	40.9%

It is also notable that the $MoSe_2$ quantum dots prepared by laser ablation for 30 min at 1.5 W exhibit overall larger PTCEs than the spherical nanoparticles prepared by laser ablation for 10 min. Quantum dots are usually considered to have lower electron relaxation rates after

excitation, as the lattice vibrations cannot couple widely separated electronic states.[50] However, much research has also found that many colloidal quantum dots with surface functionalization of ligands show much faster carrier relaxation in the timescale of picoseconds or even sub-picosecond like bulk materials thanks to non-diabatic decay channels.[51–56] Meanwhile, quantum dots can generate multiple excitons after single photon absorption.[55] The transformation of multiple excitons to single excitons can also generate heat.[55] Therefore, the higher PTCEs of the $MoSe_2$ quantum dots might be attributed to multiple electron decay channels and multiple exciton generation.

The $MoSe_2$ samples prepared in 0.5 mg/mL PEG solutions by laser ablation at 1.5 W for 30 min (quantum dots) and 10 min (spherical nanoparticles) were selected to test the stability of the PEGylated $MoSe_2$ nanomaterials. The PTCEs of these two samples were tested on Day 1, 2, 4 and 7 after preparation. The maximum temperature increase of both samples drops slightly over the storage period (**Figure 8e**), while the PTCEs of both nanomaterials are relatively stable, as shown in **Figure 8f**. The drop of the maximum temperature increase might be attributed to a slight agglomeration of the nanomaterials or the sedimentation of larger nanoparticles over time. This can be supported by the absorbance spectra of these two samples (**Figure S8**), where the absorbances of both nanomaterials slightly decline over the storage period. However, the spherical nanoparticles prepared with a shorter laser ablation time (10 min) exhibit a larger drop in the maximum temperature increase and light absorbance than the quantum dots prepared with a longer ablation time (30 min). This discrepancy could be linked to the presence of more larger nanoparticles within the sample generated with a shorter laser ablation, as all the samples were not centrifuged after preparation.

Conclusions

A one-pot synthesis method was developed to prepare PEGylated $MoSe_2$ nanomaterials by femtosecond laser ablation of $MoSe_2$ powder particles in aqueous PEG solutions. $MoSe_2$ quantum dots were synthesized by femtosecond laser ablation in PEG solutions for 30 min at 1.5 W. However, $MoSe_2$ powder could be oxidized and transformed into MoO_3 when the PEG concentration was low, like laser ablation in pure water. When the PEG concentration was higher than 0.125 mg/mL, the oxidation was suppressed. Analysis of the XPS spectra of the synthesized quantum dots unveiled peaks attributed to Mo(VI)-O bonds indicating the formation of MoO_3, as well as Mo(IV)-O bonds, likely attributed to partial oxidation or surface attachment of PEG *via* Mo-O chemical bonds. Increasing the concentration of PEG in solutions led to a reduced proportion of Mo(VI)-O bonds, suggesting that surface attachment of PEG to $MoSe_2$ quantum dots can effectively protect them from oxidation during the laser ablation process. Short-time laser ablation of $MoSe_2$ powder resulted in the formation of larger spherical nanoparticles. Although PEG molecules could be attached to the nanoparticles *via* van der Waals forces, laser ablation with higher power led to more PEG molecules attached to the nanoparticles *via* chemical bonds. It was found that surface attachment of PEG to the nanoparticles *via* chemical bonds offered better protection against oxidation into MoO_3 compared to attachment *via* van der Waals forces. Both the PEGylated $MoSe_2$ quantum dots and spherical nanoparticles exhibited high PTCEs. However, the PTCEs of the quantum dots were found to be higher than those of the larger spherical nanoparticles. This might be caused by multiple electron decay channels and multiple exciton generation. Furthermore, the laser-synthesized PEGylated $MoSe_2$ nanomaterials exhibited good PTCE stability when they were stored at room temperature. This commendable

stability, combined with high PTCEs, positions these laser-synthesized $MoSe_2$ nanomaterials as promising candidates for non-invasive cancer treatment through photothermal therapy.

ASSOCIATED CONTENT

Supporting Information.

The following files are available free of charge.

XRD patterns of nanomaterials prepared in water and PEG solutions with different concentrations. Size distributions and C1s XPS spectra of the $MoSe_2$ quantum dots and spherical nanoparticles. Tauc plots and plots to determine the Urbach energies of the $MoSe_2$ quantum dots and spherical nanoparticles. Details to calculate PTCEs of the $MoSe_2$ nanomaterials.

AUTHOR INFORMATION

Corresponding Author

* Kevin P. Musselman - Department of Mechanical and Mechatronics Engineering, University of Waterloo, Waterloo, Ontario N2L 3G1, Canada; Waterloo Institute for Nanotechnology, Waterloo, Ontario N2L 3G1, Canada.

Email: kevin.musselman@uwaterloo.ca

Author Contributions

F. Ye planned and conducted materials synthesis and characterizations. H. Fruehwald conducted Raman measurement. K. Tian assisted with the materials synthesis. M. Zandieh freeze-dried nanomaterials for characterization. The manuscript is written by F. Ye All the authors are involved in the discussion and revision of the manuscript. K. Musselman, J. Sanderson, and R. Smith supervised the work.

Funding Sources

This work is supported by the New Frontiers in Research Fund Exploration Program (NFRFE-2018-2018-00630).

ACKNOWLEDGMENT

F.Y. acknowledges Engineering Excellence Doctoral Fellowship (University of Waterloo) and W.S. Rickert Graduate Student Fellowship. F.Y. acknowledges Dr. Reza Karimi who maintained the femtosecond laser used in this work.

ABBREVIATIONS

PEG, polyethylene glycol; PTCE, photothermal conversion efficiency; NIR, near infrared; PTA, photothermal therapy agent; TMDC, transition metal dichalcogenide; PEI, polyethylene imine; PLAL, pulsed laser ablation in liquid; PVP, polyvinylpyrrolidone; TGA, thermogravimetric analysis; XPS, X-ray photoelectron spectroscopy; FTIR, Fourier transform infrared spectroscopy; ATR, attenuated total reflection.

REFERENCES

(1) Yin, W.; Yan, L.; Yu, J.; Tian, G.; Zhou, L.; Zheng, X.; Zhang, X.; Yong, Y.; Li, J.; Gu, Z.; Zhao, Y. High-Throughput Synthesis of Single-Layer MoS_2 Nanosheets As a Near-Infrared Photothermal-Triggered Drug Delivery for Effective Cancer Therapy. *ACS Nano* **2014**, *8*, 6922–6933.

(2) Feng, W.; Chen, L.; Qin, M.; Zhou, X.; Zhang, Q.; Miao, Y.; Qiu, K.; Zhang, Y.; He, C. Flower-like PEGylated MoS_2 Nanoflakes for Near-Infrared Photothermal Cancer Therapy. *Sci. Rep.* **2015**, *5*, 17422.

(3) Zhang, X.; Wu, J.; Williams, G. R.; Niu, S.; Qian, Q.; Zhu, L.-M. Functionalized MoS_2-

Nanosheets for Targeted Drug Delivery and Chemo-Photothermal Therapy. *Colloids Surf. B* **2019**, *173*, 101–108.

(4) Li, H.; Gong, M.; Xiao, J.; Hai, L.; Luo, Y.; He, L.; Wang, Z.; Deng, L.; He, D. Photothermally Activated Multifunctional MoS_2 Bactericidal Nanoplatform for Combined Chemo/Photothermal/Photodynamic Triple-Mode Therapy of Bacterial and Biofilm Infections. *Chem. Eng. J.* **2022**, *429*, 132600.

(5) Cao, W.; Yue, L.; Khan, I. M.; Wang, Z. Polyethylenimine Modified MoS_2 Nanocomposite with High Stability and Enhanced Photothermal Antibacterial Activity. *J. Photochem. Photobiol. A Chem.* **2020**, *401*, 112762.

(6) Yong, Y.; Zhou, L.; Gu, Z.; Yan, L.; Tian, G.; Zheng, X.; Liu, X.; Zhang, X.; Shi, J.; Cong, W.; Yin, W.; Zhao, Y. WS_2 Nanosheet As a New Photosensitizer Carrier for Combined Photodynamic and Photothermal Therapy of Cancer Cells. *Nanoscale* **2014**, *6*, 10394–10403.

(7) Cui, X.-Z.; Zhou, Z.-G.; Yang, Y.; Wei, J.; Wang, J.; Wang, M.-W.; Yang, H.; Zhang, Y.-J.; Yang, S.-P. PEGylated WS_2 Nanosheets for X-Ray Computed Tomography Imaging and Photothermal Therapy. *Chinese Chem. Lett.* **2015**, *26*, 749–754.

(8) Wang, J.-T.; Zhang, W.; Wang, W.-B.; Wu, Y.-J.; Zhou, L.; Cao, F. One-Pot Bottom-up Fabrication of Biocompatible PEGylated WS_2 Nanoparticles for CT-Guided Photothermal Therapy of Tumors in Vivo. *Biochem. Biophys. Res. Commun.* **2019**, *511*, 587–591.

(9) Bahadur, R.; Singh, B.; Rai, D.; Srivastava, R. Influence of PEGylation on WS_2 Nanosheets and Its Application in Photothermal Therapy. *ACS Appl. Bio Mater.* **2023**, *6*, 4740–4748.

(10) Lei, Z.; Zhu, W.; Xu, S.; Ding, J.; Wan, J.; Wu, P. Hydrophilic $MoSe_2$ Nanosheets As

Effective Photothermal Therapy Agents and Their Application in Smart Devices. *ACS Appl. Mater. Interfaces* **2016**, *8*, 20900–20908.

(11) Yuwen, L.; Zhou, J.; Zhang, Y.; Zhang, Q.; Shan, J.; Luo, Z.; Weng, L.; Teng, Z.; Wang, L. Aqueous Phase Preparation of Ultrasmall $MoSe_2$ Nanodots for Efficient Photothermal Therapy of Cancer Cells. *Nanoscale* **2016**, *8*, 2720–2726.

(12) Wang, Y.; Zhang, F.; Wang, Q.; Yang, P.; Lin, H.; Qu, F. Hierarchical $MoSe_2$ Nanoflowers as Novel Nanocarriers for NIR-Light-Mediated Synergistic Photo-Thermal/Dynamic and Chemo-Therapy. *Nanoscale* **2018**, *10*, 14534–14545.

(13) He, L.; Nie, T.; Xia, X.; Liu, T.; Huang, Y.; Wang, X.; Chen, T. Designing Bioinspired 2D $MoSe_2$ Nanosheet for Efficient Photothermal-Triggered Cancer Immunotherapy with Reprogramming Tumor-Associated Macrophages. *Adv. Funct. Mater.* **2019**, *29*, 1901240.

(14) Jia, X.; Bai, J.; Ma, Z.; Jiang, X. BSA-Exfoliated WSe_2 Nanosheets As a Photoregulated Carrier for Synergistic Photodynamic/Photothermal Therapy. *J. Mater. Chem. B* **2017**, *5*, 269–278.

(15) Moses, A. O.; Khan, M. I.; Fang, Q.; Qin, L.; Rehman, U. Z.; Zhang, Y.; Feng, D. C.; Ma, Y.; Tang, X.; Wu, C.; Adam, M. L.; Huang, D.; Liu, H.; Song, L. PVP Intercalated Metallic WSe_2 as NIR Photothermal Agents for Efficient Tumor Ablation. *Nanotechnology* **2019**, *30*, 065102.

(16) Ma, N.; Zhang, M.-K.; Wang, X.-S.; Zhang, L.; Feng, J.; Zhang, X.-Z. NIR Light-Triggered Degradable $MoTe_2$ Nanosheets for Combined Photothermal and Chemotherapy of Cancer. *Adv. Funct. Mater.* **2018**, *28*, 1801139.

(17) Wang, S.; Li, K.; Chen, Y.; Chen, H.; Ma, M.; Feng, J.; Zhao, Q.; Shi, J. Biocompatible PEGylated MoS_2 Nanosheets: Controllable Bottom-up Synthesis and Highly Efficient

Photothermal Regression of Tumor. *Biomaterials* **2015**, *39*, 206–217.

(18) Wu, C.; Wang, S.; Zhao, J.; Liu, Y.; Zheng, Y.; Luo, Y.; Ye, C.; Huang, M.; Chen, H. Biodegradable Fe(III)@WS_2 -PVP Nanocapsules for Redox Reaction and TME-Enhanced Nanocatalytic, Photothermal, and Chemotherapy. *Adv. Funct. Mater.* **2019**, *29*, 1901722.

(19) Wang, S.; Li, X.; Gong, Y.; Zhou, X.; Jin, H.; Yan, H.; Liu, J. Facile Synthesis of Soybean Phospholipid-Encapsulated MoS_2 Nanosheets for Efficient *in vitro* and *in vivo* Photothermal Regression of Breast Tumor. *Int. J. Nanomedicine* **2016**, *11*, 1819–1833.

(20) Zhang, C.; Yong, Y.; Song, L.; Dong, X.; Zhang, X.; Liu, X.; Gu, Z.; Zhao, Y.; Hu, Z. Multifunctional WS_2 @Poly(Ethylene Imine) Nanoplatforms for Imaging Guided Gene-Photothermal Synergistic Therapy of Cancer. *Adv. Healthc. Mater.* **2016**, *5*, 2776–2787.

(21) Kim, J.; Kim, H.; Kim, W. J. Single-Layered MoS_2-PEI-PEG Nanocomposite-Mediated Gene Delivery Controlled by Photo and Redox Stimuli. *Small* **2016**, *12*, 1184–1192.

(22) Liu, T.; Wang, C.; Gu, X.; Gong, H.; Cheng, L.; Shi, X.; Feng, L.; Sun, B.; Liu, Z. Drug Delivery with PEGylated MoS_2 Nano-Sheets for Combined Photothermal and Chemotherapy of Cancer. *Adv. Mater.* **2014**, *26*, 3433–3440.

(23) Yong, Y.; Cheng, X.; Bao, T.; Zu, M.; Yan, L.; Yin, W.; Ge, C.; Wang, D.; Gu, Z.; Zhao, Y. Tungsten Sulfide Quantum Dots as Multifunctional Nanotheranostics for *in vivo* Dual-Modal Image-Guided Photothermal/Radiotherapy Synergistic Therapy. *ACS Nano* **2015**, *9*, 12451–12463.

(24) Ibrahim, K. H.; Irannejad, M.; Wales, B.; Sanderson, J.; Yavuz, M.; Musselman, K. P. Simultaneous Fabrication and Functionalization of Nanoparticles of 2D Materials with Hybrid Optical Properties. *Adv. Opt. Mater.* **2018**, *6*, 1701365.

(25) Xu, Y.; Yan, L.; Li, X.; Xu, H. Fabrication of Transition Metal Dichalcogenides Quantum

Dots Based on Femtosecond Laser Ablation. *Sci. Rep.* **2019**, *9*, 2931.

(26) Wu, X.; Tian, X.; Chen, T.; Zeng, A.; Yang, G. Inorganic Fullerene-like Molybdenum Selenide with Good Biocompatibility Synthesized by Laser Ablation in Liquids. *Nanotechnology* **2018**, *29*, 295604.

(27) Moniri, S.; Hantehzadeh, M. R. Colloidal Synthesis of MoS_2 NPs by Nanosecond Laser Ablation of a Bulk MoS_2 Target in Ethylene Glycol Solution. *Opt. Quantum Electron.* **2021**, *53*, 215.

(28) Pradhan, G.; Dey, P. P.; Khare, A.; Sharma, A. K. Synthesis and Size Modulation of MoS_2 Quantum Dots by Pulsed Laser Ablation in Liquid for Viable Hydrogen Generation. *J. Appl. Phys.* **2021**, *129*, 025112.

(29) Nguyen, V.; Dong, Q.; Yan, L.; Zhao, N.; Le, P. H. Facile Synthesis of Photoluminescent MoS_2 and WS_2 Quantum Dots with Strong Surface-State Emission. *J. Lumin.* **2019**, *214*, 116554.

(30) Ye, F.; Ayub, A.; Karimi, R.; Wettig, S.; Sanderson, J.; Musselman, K. P. Defect-Rich $MoSe_2$ 2H/1T Hybrid Nanoparticles Prepared from Femtosecond Laser Ablation in Liquid and Their Enhanced Photothermal Conversion Efficiencies. *Adv. Mater.* **2023**, *35*, 2301129.

(31) Tan, D.; Zhou, S.; Qiu, J.; Khusro, N. Preparation of Functional Nanomaterials with Femtosecond Laser Ablation in Solution. *J. Photochem. Photobiol. C Photochem. Rev.* **2013**, *17*, 50–68.

(32) Tsuji, T.; Thang, D.-H.; Okazaki, Y.; Nakanishi, M.; Tsuboi, Y.; Tsuji, M. Preparation of Silver Nanoparticles by Laser Ablation in Polyvinylpyrrolidone Solutions. *Appl. Surf. Sci.* **2008**, *254*, 5224–5230.

(33) Haladu, S. A.; Elsayed, K. A.; Olanrewaju Alade, I.; Alheshibri, M.; Al Baroot, A.; Ali, S. A.; Kotb, E.; Manda, A. A.; Ul-Hamid, A.; Dafalla, H. D. M.; Drmosh, Q. A. Laser-Assisted Fabrication of Silver Quantum Dots/Polyaspartate Polymer Composite for Antimicrobial Applications. *Opt. Laser Technol.* **2022**, *152*, 108122.

(34) Choi, H.; Kim, H. S. In Situ Synthesis and Stabilization of PVP-Coated Aluminum Nanoparticles by One-Step Pulsed Laser Ablation in Liquid: Investigation and Quantification of PVP Coverage Effects. *Surfaces and Interfaces* **2023**, *43*, 103594.

(35) Sobhan, M. A.; Withford, M. J.; Goldys, E. M. Enhanced Stability of Gold Colloids Produced by Femtosecond Laser Synthesis in Aqueous Solution of CTAB. *Langmuir* **2010**, *26*, 3156–3159.

(36) Akman, E.; Aktas, O. C.; Genc Oztoprak, B.; Gunes, M.; Kacar, E.; Gundogdu, O.; Demir, A. Fragmentation of the Gold Nanoparticles Using Femtosecond Ti:Sapphire Laser and Their Structural Evolution. *Opt. Laser Technol.* **2013**, *49*, 156–160.

(37) Li, B.; Jiang, L.; Li, X.; Ran, P.; Zuo, P.; Wang, A.; Qu, L.; Zhao, Y.; Cheng, Z.; Lu, Y. Preparation of Monolayer MoS_2 Quantum Dots Using Temporally Shaped Femtosecond Laser Ablation of Bulk MoS_2 Targets in Water. *Sci. Rep.* **2017**, *7*, 11182.

(38) Ye, F.; Chang, D.; Ayub, A.; Ibrahim, K.; Shahin, A.; Karimi, R.; Wettig, S.; Sanderson, J.; Musselman, K. P. Synthesis of Two-Dimensional Plasmonic Molybdenum Oxide Nanomaterials by Femtosecond Laser Irradiation. *Chem. Mater.* **2021**, *33*, 4510–4521.

(39) Stratakis, E.; Barberoglou, M.; Fotakis, C.; Viau, G.; Garcia, C.; Shafeev, G. A. Generation of Al Nanoparticles via Ablation of Bulk Al in Liquids with Short Laser Pulses. *Opt. Express* **2009**, *17*, 12650.

(40) De Bonis, A.; Lovaglio, T.; Galasso, A.; Santagata, A.; Teghil, R. Iron and Iron Oxide

Nanoparticles Obtained by Ultra-Short Laser Ablation in Liquid. *Appl. Surf. Sci.* **2015**, *353*, 433–438.

(41) Ye, F.; Ayub, A.; Chang, D.; Chernikov, R.; Chen, Q.; Karimi, R.; Wettig, S.; Sanderson, J.; Musselman, K. P. Molybdenum Blues with Tunable Light Absorption Synthesized by Femtosecond Laser Irradiation of Molybdenum Trioxide in Water/Ethanol Mixtures. *Adv. Opt. Mater.* **2022**, *10*, 2201304.

(42) Chieng, B.; Ibrahim, N.; Yunus, W.; Hussein, M. Poly(Lactic Acid)/Poly(Ethylene Glycol) Polymer Nanocomposites: Effects of Graphene Nanoplatelets. *Polymers.* **2013**, *6*, 93–104.

(43) Zhao, X.; Sui, J.; Li, F.; Fang, H.; Wang, H.; Li, J.; Cai, W.; Cao, G. Lamellar $MoSe_2$ Nanosheets Embedded with MoO_2 Nanoparticles: Novel Hybrid Nanostructures Promoted Excellent Performances for Lithium Ion Batteries. *Nanoscale* **2016**, *8*, 17902–17910.

(44) Zhang, J.; Wu, M.; Liu, T.; Kang, W.; Xu, J. Hierarchical Nanotubes Constructed from Interlayer-Expanded $MoSe_2$ Nanosheets as a Highly Durable Electrode for Sodium Storage. *J. Mater. Chem. A* **2017**, *5*, 24859–24866.

(45) Bhatt, S.; Pulpytel, J.; Mirshahi, M.; Arefi-Khonsari, F. Catalyst-Free Plasma-Assisted Copolymerization of Poly(ε-Caprolactone)-Poly(Ethylene Glycol) for Biomedical Applications. *ACS Macro Lett.* **2012**, *1*, 764–767.

(46) Dobrea, I. D.; Ciocan, C. E.; Dumitriu, E.; Popa, M. I.; Petit, E.; Hulea, V. Raman Spectroscopy — Useful Tool for Studying the Catalysts Derived from Mo and V-Oxyanion-Intercalated Layered Double Hydroxides. *Appl. Clay Sci.* **2015**, *104*, 205–210.

(47) Kumari, L.; Ma, Y.-R.; Tsai, C.-C.; Lin, Y.-W.; Wu, S. Y.; Cheng, K.-W.; Liou, Y. X-Ray Diffraction and Raman Scattering Studies on Large-Area Array and Nanobranched

Structure of 1D MoO_2 Nanorods. *Nanotechnology* **2007**, *18*, 115717.

(48) Tang, J.; Wei, Z.; Wang, Q.; Wang, Y.; Han, B.; Li, X.; Huang, B.; Liao, M.; Liu, J.; Li, N.; Zhao, Y.; Shen, C.; Guo, Y.; Bai, X.; Gao, P.; Yang, W.; Chen, L.; Wu, K.; Yang, R.; Shi, D.; Zhang, G. In Situ Oxygen Doping of Monolayer MoS_2 for Novel Electronics. *Small* **2020**, *16*, 2004276.

(49) Wei, Z.; Tang, J.; Li, X.; Chi, Z.; Wang, Y.; Wang, Q.; Han, B.; Li, N.; Huang, B.; Li, J.; Yu, H.; Yuan, J.; Chen, H.; Sun, J.; Chen, L.; Wu, K.; Gao, P.; He, C.; Yang, W.; Shi, D.; Yang, R. Zhang, G. Wafer-Scale Oxygen-Doped MoS_2 Monolayer. *Small Methods* **2021**, *5*, 2100091.

(50) Pandey, A.; Guyot-Sionnest, P. Slow Electron Cooling in Colloidal Quantum Dots. *Science.* **2008**, *322*, 929–932.

(51) Schaller, R. D.; Klimov, V. I. High Efficiency Carrier Multiplication in PbSe Nanocrystals: Implications for Solar Energy Conversion. *Phys. Rev. Lett.* **2004**, *92*, 186601.

(52) Kilina, S. V.; Kilin, D. S.; Prezhdo, O. V. Breaking the Phonon Bottleneck in PbSe and CdSe Quantum Dots: Time-Domain Density Functional Theory of Charge Carrier Relaxation. *ACS Nano* **2009**, *3*, 93–99.

(53) Cooney, R. R.; Sewall, S. L.; Anderson, K. E. H.; Dias, E. A.; Kambhampati, P. Breaking the Phonon Bottleneck for Holes in Semiconductor Quantum Dots. *Phys. Rev. Lett.* **2007**, *98*, 177403.

(54) Schaller, R. D.; Pietryga, J. M.; Goupalov, S. V.; Petruska, M. A.; Ivanov, S. A.; Klimov, V. I. Breaking the Phonon Bottleneck in Semiconductor Nanocrystals via Multiphonon Emission Induced by Intrinsic Nonadiabatic Interactions. *Phys. Rev. Lett.* **2005**, *95*,

196401.

(55) Hyeon-Deuk, K.; Prezhdo, O. V. Photoexcited Electron and Hole Dynamics in Semiconductor Quantum Dots: Phonon-Induced Relaxation, Dephasing, Multiple Exciton Generation and Recombination. *J. Phys. Condens. Matter* **2012**, *24*, 363201.

(56) Knowles, K. E.; McArthur, E. A.; Weiss, E. A. A Multi-Timescale Map of Radiative and Nonradiative Decay Pathways for Excitons in CdSe Quantum Dots. *ACS Nano* **2011**, *5*, 2026–2035.

Table of Contents